ELSEVIER

Polymer 40 (1999) 6897–6909

polymer

Contribution of amylose and amylopectin to the light scattering behaviour of starches in aqueous solution

P. Roger*, L.A. Bello-Perez[1], P. Colonna

Institut National de la Recherche Agronomique, 44316 Nantes Cedex 03, France

Received 9 June 1998; received in revised form 5 January 1999; accepted 5 January 1999

Abstract

Investigations based on static and dynamic light-scattering studies were conducted to assess the influence of amylose content (0.0–65.8%) and microwave dispersion treatment (MDT) on the macromolecular features of starches, including fractal behaviour. Values for apparent average molar mass ($\bar{M}_W$), gyration radius ($\bar{R}_G$) and hydrodynamic radius ($\bar{R}_H$) were obtained using common extrapolation procedures to the zero scattering vector. The general trend showed a decrease in these values when amylose level or the intensity of MDT was increased. However, unexpected results were obtained, mainly for the starch with the highest amylose content and for long MDT times. The high $\mathbf{q}\bar{R}_G$-range [where $\mathbf{q}$ is the scattering vector; $\mathbf{q} = (4\pi n/\lambda)sin(\theta/2)$] allowed the internal behaviour of starch samples to be studied as well. Kratky plots, fractal dimensions, and relaxation rate dependence on $\mathbf{q}$ revealed significant differences in internal structures and the influence of amylose content. At low amylose contents (0.0–28.5%), light-scattering behaviour was dominated by the amylopectin contribution, in agreement with Galinski and Burchard (Macromolecules 1995;28:2363), whereas at high amylose contents (52.5–65.8%), light-scattering behaviour was influenced by amylose despite the high dimensions of amylopectin.

Keywords: Starch; Light scattering; Macromolecular characterization

1. Introduction

Starch, the major storage polysaccharide in higher plants, is a mixture of two macromolecular α-glucans, one essentially linear (amylose) and the other highly branched (amylopectin). The various structural elements of these macromolecules, such as polydispersity, overall molecular dimensions, hydrodynamic behaviour and internal mobility, exert a marked influence on their properties in solution [1–3].

Starch owes all its functionalities to these macromolecules as well as to their physical organisation into native semi-crystalline granules [4]. Starch is widely utilised in many applications for which the first step is generally a dispersion, carried out in non-degradative conditions. The resulting pastes can be used for their thickening, gelling, and/or stabilising properties [5–8].

Similarly, for the characterisation of amylose and amylopectin, starch granules need to be completely destructured without breaking the macromolecule structure. Recently, optimal conditions have been found through pre-treatment of samples with 95% dimethylsulphoxide (DMSO), followed by a dissolution step using microwave dispersion treatment (MDT) [9].

Very few studies have been devoted to the relationships between the fine structure of these molecules and their behaviour in solution. Thurn and Burchard [2] were the first to propose a combination of static (SLS) and dynamic light scattering (DLS) in studies of the structure and properties of native, non-degraded starch components. DLS is based on the scattering of light by moving particles [10]. At any given time (time scale μs), the suspended particles of molecules assume a particular set of positions within the scattering volume. These particles scatter radiation to the detector with differing incident phases due to their relative spatial positions and different particle–detector distances. In SLS, the intensity of scattered radiation is averaged over a fairly long time ($\approx$2 s), which is in most cases sufficient to smooth out all internal mobility [11]. For $\mathbf{q}\bar{R}_G < 1$, SLS provides useful information, such as the weight-average molar mass, $\bar{M}_W$ the root-mean-square z-average radius of gyration, $\bar{R}_G$, and the light-scattering second osmotic virial coefficient, A_2, of macromolecules in dilute solution [12].

Aberle et al. [13] used a light-scattering technique to obtain the $\bar{M}_W$ and $\bar{R}_G$ of various species of starch. An interesting mathematical analysis of data also enabled

* Corresponding author.

[1] Present address: Instituto Tecnológico de Acapulco, Apartado Postal 600 C.P. 39300 Acapulco, Guerrero, Mexico.

0032-3861/99/$ - see front matter
PII: S0032-3861(99)00051-8

these authors to calculate the $\bar{M}_W$ and $\bar{R}_G$ of each starch component. For amylopectin, molar masses of 60×10^6–110×10^6 g/mol and radii around 220 nm were found, whereas unexpected low values of $\bar{R}_G$ (between 19 and 60 nm), as compared to $\bar{M}_W$ values (2.1×10^6–2.0×10^7 g/mol), were noted for amylose. This was interpreted as lateral (side-by-side) aggregation of the amylose chains, with reference to the so-called fringed micelle structure [14]. Owing to the large size of amylopectin, light scattering should be used to probe internal structures and characterise molecular segments with dimensions greater than 10 nm. Using SLS and DLS techniques, Galinsky and Burchard [1,15] studied the dimensional properties and behaviour, in solution, of starch fractions of different molar masses prepared by acid degradation of potato starch. At this low level of amylose content (normal potato starch generally contains less than 22% of amylose), light-scattering behaviour was dominated by the amylopectin part. Their results are in good agreement with the theoretical model of ABC polycondensation. However, the discrepancy between the obtained segment density (0.016) and the value determined by nuclear magnetic resonance and enzymatical techniques (0.04) remains unexplained.

Recently, molar mass distributions of starches have been obtained by sedimentation field flow fractionation (SdFFF) [16,17]. Waxy corn and potato starches can be fractionated by the SdFFF technique within a broad range of R_G (50–500 nm), allowing better amylopectin characterisation. With this technique, the analysis of measured particle scattering factors, $P(q)$, has provided information about the structural properties of amylopectin molecules to be obtained from a single starch sample as a function of relative molecular weight. Self-similar structures have been observed, with fractal dimensions of 2.4 ± 0.1. Only small differences in the internal structures of waxy corn and potato starches have been noted, with potato starch appearing only slightly more expanded than waxy corn starch.

To date, one common result of all chromatographic studies of starch is that amylose and amylopectin cannot be strictly separated on the basis of their respective sizes in solution. All fractionation procedures [3,9] based on complexation lead to intermediate fractions between amylose and amylopectin, which suggests a continuous change between these two well-identified chemical species. Thus, analysis of starch as a single α-glucan should indicate whether amylose or amylopectin makes the major contribution to the features and behaviour relative to the amylose/amylopectin ratio.

As these recent studies have mainly concerned starches with high amylopectin contents, it seemed of interest to undertake a systematic study of the effects of increasing amylose content on light-scattering behaviour. More precisely, the present study sought to characterise the dimensions and structural properties of two high-amylose and two high-amylopectin starches after solubilisation by MDT. Through application of light-scattering techniques, the high $\mathbf{q}\bar{R}_G$-range used in these studies facilitated investigation of the internal structure. Another advantage is that this $\mathbf{q}\bar{R}_G$-range is the same as that used in an on-line multi-angle light scattering detector. In recent years, this detector has provided the most reliable and rapid characterisation of polymers in solution, even for starch [9,16]. When applied to polymers with huge molar masses, the common extrapolation procedure to the zero scattering vector should be used with caution owing to the high $\mathbf{q}\bar{R}_G$-range. Another aim of this study was to assess the suitability of different ways of processing experimental data.

2. Materials and methods

2.1. Sample preparation

The high amylopectin starches used were corn amylopectin (sample A) (Sigma, St. Louis, MO), and normal corn starch (sample B) (Roquette Frères, Lestrem, France). High-amylose starches were obtained from Eurylon 5® (sample C) and Eurylon 7® (sample D). Starches (1 g) were first dissolved in 95% DMSO (20 ml), with magnetic stirring for 3 days at room temperature. The sample was then precipitated with ethanol (60 ml) and stored overnight at 4°C. The precipitate was filtered over a glass filter (G4), washed successively with acetone (10 ml) and diethyl ether (10 ml), air-dried under a hood for a few hours to eliminate solvents, and finally dried in vacuo at 45°C for 18–24 h.

2.2. Sample solubilisation

The solubilisation procedure was initiated by the addition of water (20 ml), previously filtered through 0.1 μm (Anotop, Whatmann, Maidstone, UK), to a dried dispersed starch sample (10 mg), previously weighed in the Teflon cup of a model 4782 polycarbonate microwave bomb (total volume 45 ml) (Parr Instrument Co., Moline, IL, USA). The sample was maintained for 15 min under nitrogen flow before the capped Teflon cup was fitted into the bomb, which had its own pressure cap. This assembly was centred inside a 900 W Panasonic microwave oven NN-5252B (Panasonic, Matsushita Electric Industrial Co., Osaka, Japan). The sample was heated for 35 s (143°C), 50 s (177°C), 70 s (201°C) and 90 s (211°C) at 900 W, and the maximum temperature (in brackets) was recorded inside a home-made Teflon cup using an optic fibre. A cooling step was carried out by immersion in an ice-bath for 30 min, and the sample was then centrifuged at 31 200*g* for 10 min at 20°C. The supernatant solution was filtered through 5 μm (Millipore, Bedford, MA) directly into the scattering cell and immediately analysed. The dilution series was performed at room temperature, yielding four lower concentrations. The carbohydrate concentrations of the supernatant solution after filtration, and of each of the successive

Table 1
Macromolecular features of corn amylopectin and starch samples dissolved by microwave heating at different times. $\bar{M}_W$ = molar mass, g/mol; $\bar{R}_G$ = gyration radius, nm; $\bar{R}_H$ = hydrodynamic radius, nm; $\rho = \bar{R}_G/\bar{R}_H$; d_f = fractal dimension (e.g. slopes of log $R(\mathbf{q})$ vs. log $\mathbf{q}$)

Sample	Heating time (s)	Solubilisation extent (%)	$\bar{M}_W \times 10^{-7}$	$\bar{R}_G$	$\bar{R}_H$	ρ	d_f
A	35	88.6	27	259	201	1.29	2.20
A	50	92.6	24	260	221	1.18	2.12
A	70	97.5	11	190	187	1.02	1.95
A	90	100.0	7.8	170	148	1.15	1.80
B	35	94.7	25	267	201	1.33	2.28
B	50	96.2	16	230	207	1.11	2.10
B	70	100.0	3.6	134	135	0.99	1.51
B	90	100.0	0.9	131	99	1.32	1.00
C	35	97.6	3.1	172	127	1.35	1.69
C	50	98.7	2.8	158	124	1.27	1.59
C	70	100.0	2.0	134	122	1.10	1.38
C	90	100.0	0.8	182	185	0.98	1.46
D	35	97.5	2.3	187	139	1.35	1.55
D	50	100.0	2.0	180	116	1.55	1.50
D	70	100.0	1.4	158	98	1.61	1.32
D	90	100.0	1.3	187	153	1.22	1.49

dilutions, were measured by the sulphuric acid–orcinol colorimetric method [18].

2.3. Static light scattering

Experiments were performed at 25°C in the angular range from 30 to 150° in 15° steps in homodyne mode with full photon-counting detection using a 128-channel K7025 Malvern correlator. Incident radiation at 514.5 nm was obtained from a vertically polarised 3 W Ar Ion Spectra-Physics laser. The refractive index increment (dn/dc) was taken as 0.146 ml/g [19]. Optical alignment was checked over the angular range described using benzene filtered through 0.02 μm Anotop® membranes. The value of the corresponding Rayleigh ratio for benzene at 514.5 nm was $5.5 \times 10^{-5}\,\mathrm{cm}^{-1}$. Monitoring programs were written in BASIC and run on an HP9300 microcomputer. All fitting was performed using a Berry plot with a home-made program.

2.4. Dynamic light scattering

Measurements were made with an ALV-5000 correlator (ALV-Laser, Vertriebsgesellschaft mbH., Lagen, Germany) in the angular range from 30 to 150° in 30° steps using the previous equipment. Two different methods were applied to process the data: (i) cumulant analysis (using ALV-5000 software, Version 5.0) to construct the dynamic Zimm plots and (ii) inverse Laplace transformation (ILT) (where $g_1(t) = \int_0^\infty A(\tau)\exp(-t/\tau)\mathrm{d}\tau$ and $A(\tau)$ is the distribution function of decay times τ) to obtain the distribution of relaxation times from the measured autocorrelation functions.

The GENDIST® program written by Bob Johnsen (Uppsala University, Sweden), is based upon a constrained

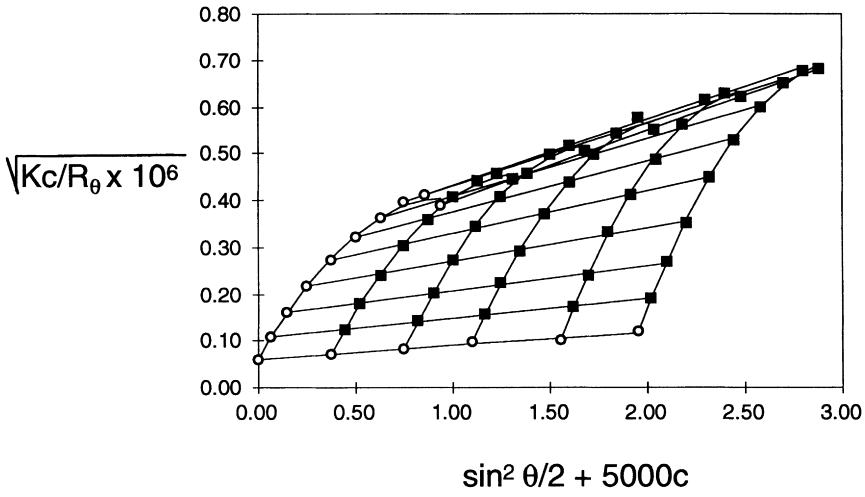

Fig. 1. Berry plot obtained for normal corn starch in water at 25°C.

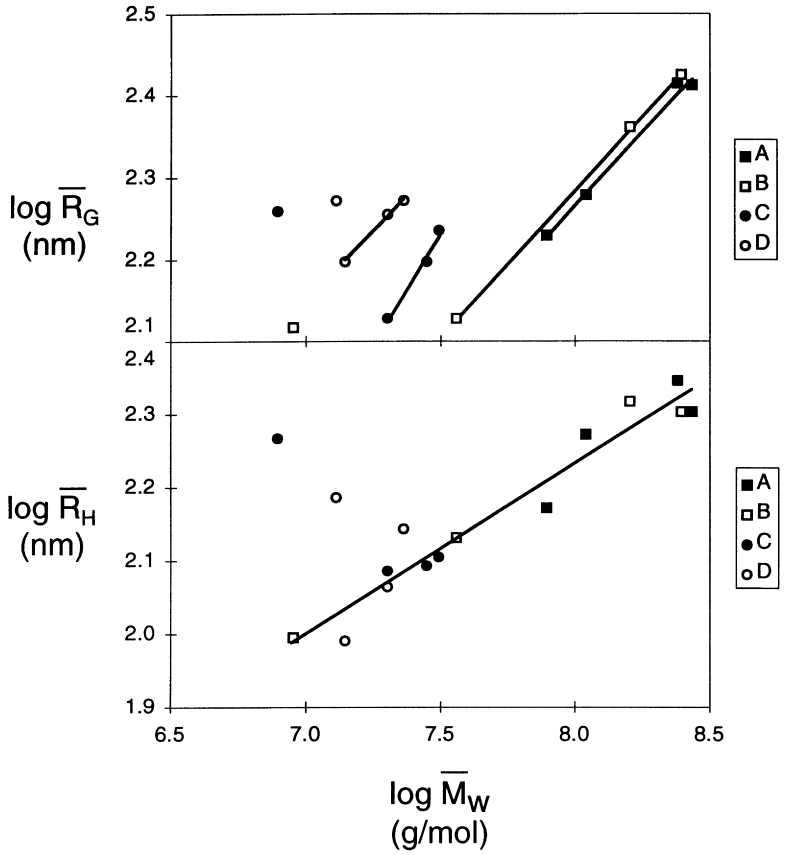

Fig. 2. Log–log plots of the $\bar{M}_W$ dependence of $\bar{R}_G$ and $\bar{R}_H$ of starch samples treated using MDT for different times.

regularisation algorithm, denoted REPES, which gives results similar to the CONTIN inversion routine. However, REPES directly minimises the sum of the squared differences between experimental and calculated $g_2(t)$ functions, by using an equidistant logarithmic grid of fixed components, and determines their amplitudes [20]. A grid of 30 per decade was used here to obtain a smoothed distribution suitable to the broad polydisperse distributions expected for starch.

3. Results and discussion

Starches A, B, C and D gave a wide range of amylose content: 0.0, 28.5, 52.5 and 65.8%, respectively, as determined by their respective iodine-binding capacities. These samples were treated for different time periods (35, 50, 70 and 90 s) in the microwave bomb and then immediately characterised by SLS and DLS.

3.1. Static light scattering

3.1.1. Molecular degradation

As the Zimm plot procedure did not allow sufficiently accurate extrapolation to the zero scattering angle for molecules of high molar mass (even negative molar masses can be obtained, Ref. [13]), molar masses $\bar{M}_W$ and radii of gyration $\bar{R}_G$ (Table 1) were measured by SLS and processed using a Berry plot with a second-order polynomial fit for angular dependence (Fig. 1).

For an MDT treatment time of 35 s, $\bar{M}_W$ and $\bar{R}_G$ values for samples A, B, C and D were, respectively, 2.7×10^8 g/mol and 259 nm; 2.5×10^8 g/mol and 267 nm; 3.1×10^7 g/mol and 172 nm; and 2.3×10^7 g/mol and 187 nm. These features characterised two groups of starch samples: amylopectin-rich starches, i.e. samples A and B, for which $\bar{M}_W$ and $\bar{R}_G$ were approximately 10 times and 3/2 times as high as the values of amylose-rich starches, i.e. samples C and D, respectively.

At this point, it is interesting to apply the relationship of additivity of the weight-average molar mass to starch:

$$\bar{M}_W = (1 - x)\bar{M}_{W,amp} + x\bar{M}_{W,amy} \quad (1)$$

where x is the weight fraction of amylose, and $\bar{M}_W$, $\bar{M}_{W,amp}$ and $\bar{M}_{W,amy}$ are the weight-average molar masses of starch, amylopectin and amylose, respectively.

Previous works [21–23] have shown that $\bar{M}_{W,amy}$ for corn starches are always lower than 5×10^5 g/mol. Consequently the second term $x\bar{M}_{W,amy}$ in Eq. (1) represents less than 1% of the total $\bar{M}_W$, reported in Table 1 for 35 s of MDT. So total $\bar{M}_W$ can be used to calculate an approximation of $\bar{M}_{W,amp}$, neglecting the contribution of amylose. The

Table 2
Exponents of the scaling relationships for samples analysed by laser light scattering. ν_{R_G} and ν_{R_H} were obtained from the slope of M_W vs. R_G or R_H

Sample	ν_{R_G}	ν_{R_H}
A	0.36	0.25
B	0.37	0.23
C	0.60	0.23
D	0.30	0.66

discrepancy between the calculated value (1.9×10^8 g/mol) and the experimental value (2.5×10^8 g/mol) lies within the experimental error for B. Samples C and D present similar values for $\bar{M}_{W,amp}$, 6.5×10^7 and 6.7×10^7 g/mol, respectively. Two important conclusions can be drawn. $\bar{M}_{W,amp}$ are significantly depending upon the amylose content, i.e. genotypes. Total $\bar{M}_W$, can be used to calculate $\bar{M}_{W,amp}$, without having recourse to long and tedious starch fractionation.

For a fixed amount of amylose content, the general trend was a decrease of $\bar{M}_W$ and $\bar{R}_G$ when microwave heating time increased, which was indicative of a degradation of starch components for long treatment periods. However, $\bar{R}_G$ values for starches C (182 nm) and D (187 nm), heated for 90 s, increased slightly compared to samples treated for shorter periods, possibly because of poor stability in solution at a temperature of 25°C for amylose. This trend, i.e. an increase in $\bar{R}_G$ values as $\bar{M}_W$ decreased, has already been observed [24].

3.1.2. Molar mass dependence of the radius of gyration

Using the average values of $\bar{M}_W$ and $\bar{R}_G$, a first investigation was conducted concerning the preservation of the initial primary structure of the different samples during microwave dispersion. Fig. 2 shows the $\bar{M}_W$ dependences of $\bar{R}_G$ on a double logarithmic plot for the different samples, A–D, for the four treatment times. The data points corresponding to samples A and B follow approximately the same straight line, except for the last point of B. Subsequently, as amylose content increases (i.e. samples C and D), the data points are shifted to lower molar masses, and two other straight lines can be observed crossing, respectively, the first three points of samples C and D. The points corresponding to the longer treatment time (90 s) are not on these lines since the value of $\bar{R}_G$ was too high. Thus, by using the four experimental points for A and only the first three points of the process for B, C and D, four different straight lines were obtained, giving power law relationships of the type

$$\bar{R}_G \sim \bar{M}^{\nu_{R_G}} \quad (2)$$

Exponents ν_{R_G}, calculated from the slopes of these straight lines, were between 0.30 and 0.60 (Table 2). The close ν_{R_G} values obtained for A and B, 0.36 and 0.37 respectively, were between the ν_{R_G} value of 0.33 characteristic of a hard sphere and another comparable value of 0.39 on a similar structure, i.e. potato starch samples degraded by acid treatment [1]. It can be concluded from these values that the initial highly branched structure of samples A and B was roughly preserved during the solubilisation process.

In the same manner, the exponent $\nu_{R_G} = 0.6$ obtained for C was related to the high linear chain content (~52.5%) of this sample. However, the exponent of 0.3 obtained for D was too low to be explained in the same way as the amylose content, i.e. the amount of linear chain was highest (65.8%) in this sample. The ν_{R_G} value can hardly be explained on the basis of a simple model involving a mixture of non-interacting linear and highly-branched structures. In this model, it is not possible to obtain a lower value than the one expected for a hard sphere, $\nu_{R_G} = 0.33$. Another phenomenon leading to a more compact structure (~microgel) might have occurred, which could be related either to the presence of intermediate material created by the MDT process or the instability of amylose chains at 25°C, leading to inter- and/or intra-chain associations during cooling after the MDT process.

Values of the ν_{R_G} coefficients need to be confirmed for two main reasons. Firstly, too few of data points are available to establish the power-law relationships. Secondly, the

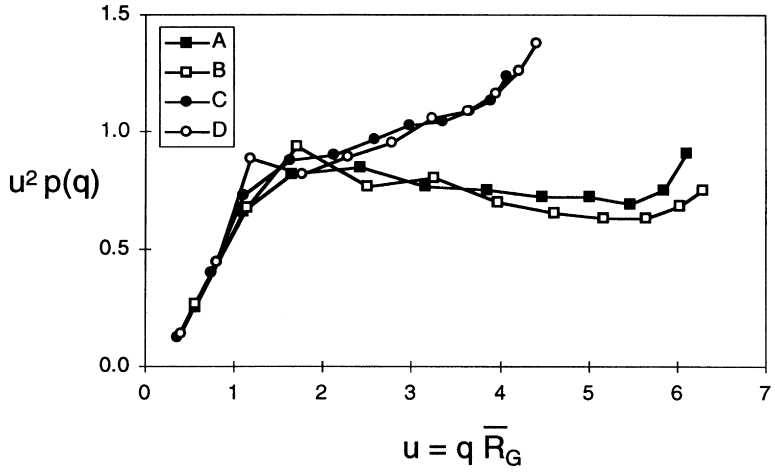

Fig. 3. Kratky plot of samples dissolved at 35 s: (a) sample A, (b) sample B, (c) sample C and (d) sample D.

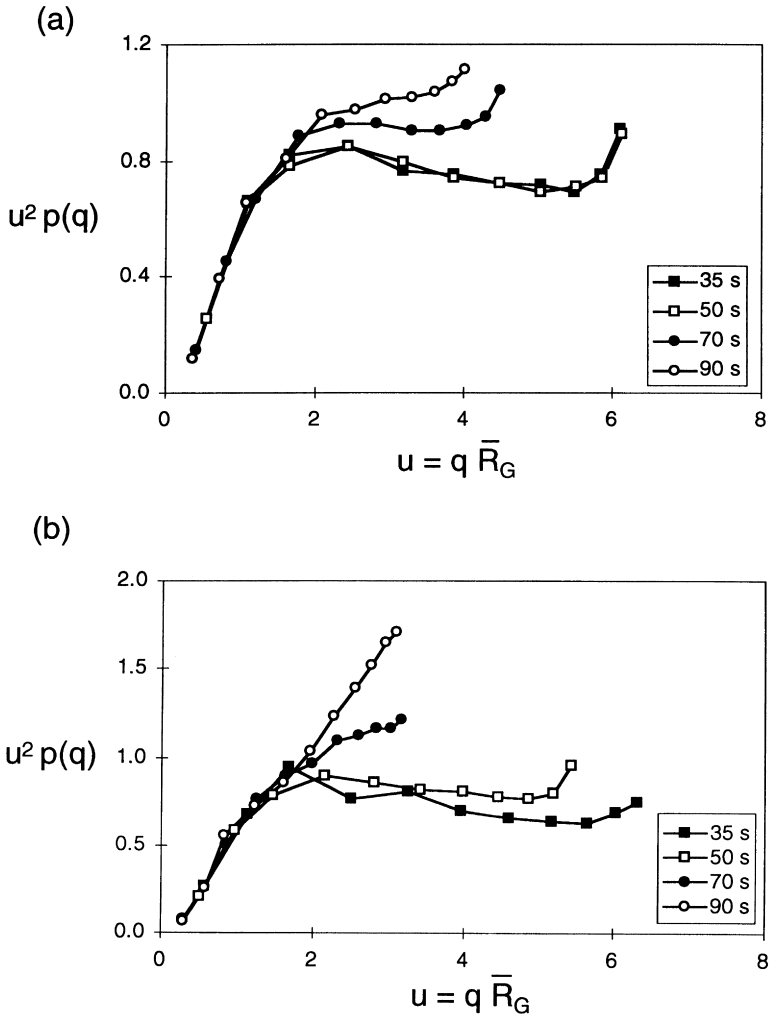

Fig. 4. Kratky plot of samples treated using MDT for different heating times: (a) sample A, (b) sample B, (c) sample C, and (d) sample D.

polydispersity of the starch samples is not taken into account when Eq. (2) is used, which can induce an error on the determination of ν_{R_G}. It would be more appropriate to use, instead of the *z*-average radius of gyration ($\bar{R}_G = \bar{R}_{Gz}$), the weight-average radius of gyration ($\bar{R}_{Gw}$) which is not found using SLS. Further work is in progress to solve these problems.

In fact, the important result is that the $\bar{R}_G$ dependence on $\bar{M}_W$ follows different trends depending on the amylose content (Fig. 2). As the amylose content increases, the log–log $\bar{R}_G = f(\bar{M}_W)$ relationships are shifted to higher molar mass values. For a fixed $\bar{R}_G$ value, the molar mass increases in the following order D < C < B ≤ A, meaning that starch sample D is less dense than C, which in turn is less dense than B, which is approximately similar in structural density to A.

3.1.3. Kratky plots

The influence of both amylose content and treatment time on the macromolecular features of starch was investigated by applying Kratky plots. As recently stated by others [13], the common range of **q**-values used in light-scattering experiments and the large radii of gyration of starch samples give increased interest to this kind of processing. In this approach, the particle-scattering factor ($P(q)$), multiplied by u ($\cong \mathbf{q}R_G$) squared, is plotted against u. Fig. 3 shows the Kratky plots of samples A–D at 35 s of treatment time, at which no degradation of samples is expected. The response of the four starch materials was the same at low $u = \mathbf{q}R_G$ (0–1.5), but differed at high u values. No plateau region is observed. In the asymptotic region (i.e. at u values higher than 2), which reflects the internal structure, even small changes in the particle-scattering factor can be observed [14,17]. The behaviour at high u values led to marked differences between the two low amylose samples A and B and the two high amylose samples C and D. No marked difference occurred for low amylose samples A and B, whereas the shapes of the Kratky plots were the same for high amylose samples C and D. Although a maximum at $u =$ 1.5–2.5, followed by a steady decrease of the function ($u^2p(\mathbf{q})$) for higher u values, was observed for samples A and B, a constant increase of the ($u^2p(\mathbf{q})$) function was

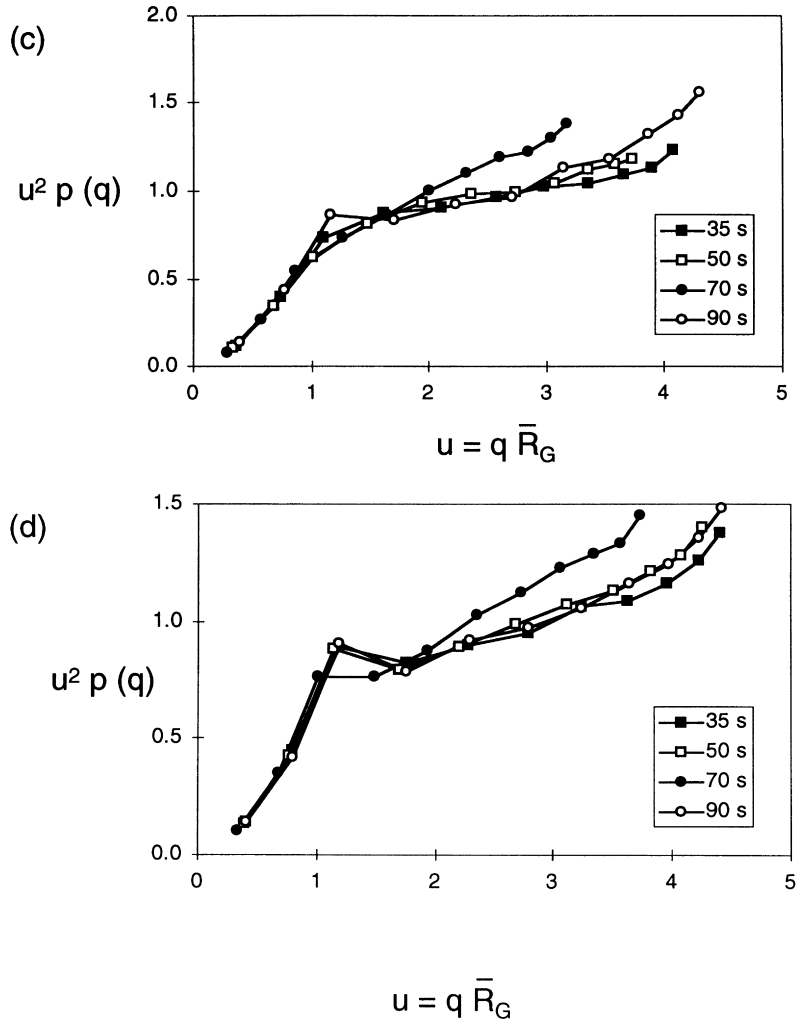

Fig. 4. (*continued*)

obtained for samples C and D. Thus, a clear difference in the internal structures of high- and low-amylose samples was observed with Kratky plots.

The effect of treatment time was considered separately for each of the samples studied (Fig. 4(a)–(d)). The general trend for these curves is that a longer treatment time leads to a greater ($u^2p(\mathbf{q})$) function increase as u becomes larger. This change reflects a global increase in linearity which could be interpreted as an effect of statistical macromolecular degradation. There is a decrease in the branching density due to the formation of small linear chains.

For high-amylose C and D starches, the values for samples treated for 90 s decreased slightly as compared to those for samples treated for 70 s. An aggregation of amylose chains reaching the dissolving gap [25] at this degradation time could account for the increase in compactness.

In the two analyses of SLS data described above, $\bar{M}_W$ and $\bar{R}_G$ were used despite great uncertainty concerning extrapolation to the zero scattering vector in the high **q** range under study. However, the slight difference from the previously reported apparent $\bar{M}_W$ and $\bar{R}_G$ values obtained by SEC-MALLS for the same starch samples processed for the initial treatment time (35 s) [9] indicates that both techniques give reliable results.

3.1.4. Fractal dimension d_f

This approach makes it possible to obtain macromolecular features without knowing $\bar{M}_W$ and $\bar{R}_G$. Information about the structure of polymers can be obtained from the dependence of the particle-scattering function $P(\mathbf{q}) = R(\mathbf{q})/R(\mathbf{q} = 0)$ on the scattering vector **q**. $P(\mathbf{q})$ describes the angular distribution of the scattered light. The theory of fractals [26] relates the asymptotic slope at high **q**-values to a fractal dimension. d_f characterises the intrinsic structure.

The fractal dimensions (d_f) are obtained directly from the slope of the asymptote at high **q** on the log–log plot of $R(\mathbf{q})$ vs. **q**; $R(\mathbf{q} = 0)$ is a constant for one experiment. Another advantage of using this method is that a fractal dimension is obtained for each sample at each treatment time. In fact, these slopes showed dependence on amylose content as well as treatment time.

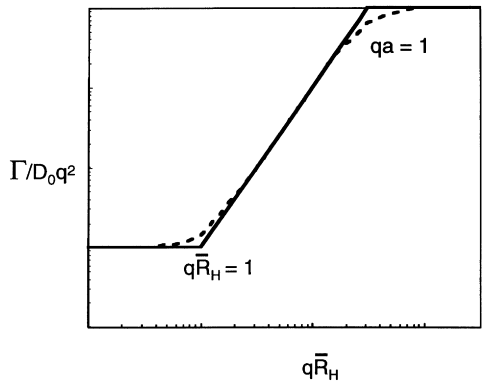

Fig. 5. Schematic image of the normalised relaxation rate $\Gamma/D_0\mathbf{q}^2$ vs. $\mathbf{q}\bar{R}_H$. Adapted from Ref. [30].

The influence of amylose content on d_f obtained at 35 s will be considered first (Table 1). For these non-degraded samples, a marked difference occurred once again between low and high amylose starches. Slight differences were found in d_f values between samples A (2.20) and B (2.28). These d_f values were between those of the fractal dimension predicted by the percolation theory [27] for non-swollen crosslinked clusters (~theta solvent) ($d_f = 2.5$) and those of fully swollen clusters (~thermodynamically good solvent) ($d_f = 2.0$). Slightly higher values of 2.44 (waxy corn) and 2.38 (potato) for d_f were obtained [17] using SdFFF-MALLS. The values obtained for C and D were 1.69 and 1.55, respectively, which are characteristic of linear structures. The value obtained for C was exactly that expected theoretically for a random coil in good solvent. The decrease observed for D could have been due to an increase in the stiffness of the structure as $d_f = 1.0$ would be likely for a rigid rod. A marked trend was the general decrease of d_f as treatment time increased (Table 1). However, the d_f value for C and D starches treated for 90 s increased only slightly.

The decrease in d_f at each amylose content shall now be considered in greater detail. For A, the values were 2.20, 2.12, 1.95 and 1.80, for 35, 50, 70 and 90 s of treatment time, respectively. This decrease could be interpreted as an expansion of the excluded volume occupied by the polymers, i.e. a better solubility as the molar mass decreases. However, the 1.80 value (90 s) was out of the range of systematic error (±0.02) and cannot be interpreted in this manner. Probable leakage of linear chains released from the weakly branched domain of amylopectin could account for the drop in the value of d_f. For B, the decrease in d_f was even more marked, from 2.28, 2.10 and 1.51 down to 1.00, indicating a higher degradation of the internal structure. At the final treatment time, the value 1.00 was characteristic of high stiffness.

The d_f values for C and D exhibited similar trends with treatment time, i.e. a decrease of d_f values from 1.69 and 1.56 down to 1.36 and 1.35 (Table 1). These values are characteristic of linear internal structures, which are strengthened as treatment time increases. The samples at 90 s showed slight increases in d_f values: this tendency was unexpected and could not be explained.

3.2. Dynamic light scattering

In DLS, the measured relaxation rate Γ is related to $\mathbf{q}\bar{R}_H$, with an exponent depending on the dynamic regime occurring. Fig. 5 shows the different dynamic regimes observed, depending on the value of $\mathbf{q}\bar{R}_H$. In the regime $\mathbf{q}\bar{R}_H < 1$, Γ equals $D_0\mathbf{q}^2$, where D_0 is the translational diffusion coefficient. The hydrodynamic radius $\bar{R}_H$ may then be calculated from D_0 using the Stokes–Einstein relationship:

$$\bar{R}_H = k_B T/(6\pi\eta_0 D_0) \quad (3)$$

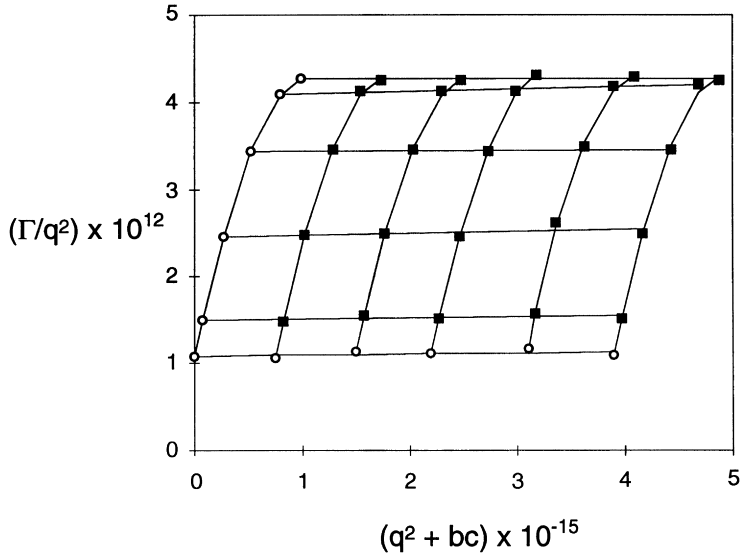

Fig. 6. Dynamic Zimm plot obtained for corn amylopectin in water at 25°C.

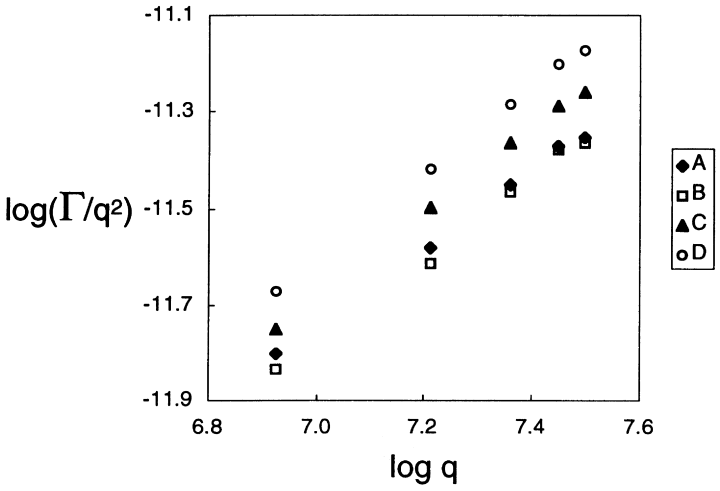

Fig. 7. Log–log plot of the first relaxation rate, $\Gamma/\mathbf{q}^2$ vs. the scattering vector, $\mathbf{q}$.

where k_B is the Boltzmann constant, T the temperature and η_0 the solvent viscosity. At $\mathbf{q}\bar{R}_H \approx 1$, a crossover (which generally spans an order of magnitude in $\mathbf{q}$) is expected to occur to the regime, where $\Gamma \sim \mathbf{q}^3$. In this intermediate regime, where $\mathbf{q}a \ll 1 \ll \mathbf{q}R$, Γ is sensitive to internal dynamics, a is the segment length of the monomer unit. Finally, when $\mathbf{q}a = 1$, a crossover is expected to diffusional motion of individual monomers, i.e. D_m (the monomer diffusion constant). The high-$\mathbf{q}$ regime, in which monomer diffusion dominates, is not suited for light-scattering studies as the condition $\mathbf{q}a \approx 1$ cannot be achieved.

3.2.1. Hydrodynamic radius

Owing to the high $\mathbf{q}\bar{R}_G$-range (calculated with the $\bar{R}_G$ values from Table 1) used in this study (between 0.8 and 6.3), it would not normally be possible to obtain hydrodynamic radii values ($\bar{R}_H$) for the starch samples by direct use of a dynamic Zimm plot, which consists in the extrapolation of the apparent diffusion coefficient $D_{app} = \Gamma/\mathbf{q}^2$ (where Γ, the first-order relaxation rate, is obtained from cumulant analysis) to the zero scattering vector and concentration. However, the high quality of the diagram permitted this type of plot. Fig. 6 shows an example of a dynamic Zimm plot obtained for sample A at 35 s. A second-order fit was used for angular extrapolation because of the considerable curvature observed at high $\mathbf{q}$ values. If the effect of amylose content on the results of undegraded samples is considered, $\bar{R}_H$ values appear to be equal for the two low amylose A and B starches (201 nm) and are much lower for the two high amylose C and D starches (127 and 139 nm, respectively).

When treatment time increased, $\bar{R}_H$ decreased for all starch samples, reflecting macromolecular degradation during the process. However, for C and D at the last treatment time (90 s), $\bar{R}_H$ increased to higher values than those obtained at the initial treatment time of 35 s, indicating a possible aggregation of the degraded amylose chains as soon as the degree of polymerisation was close to the dissolving gap.

The same processing was used as for the molar mass dependence of $\bar{R}_G$ in order to find the exponent ν_{R_H} in the power law $\bar{R}_H \sim \bar{M}_W^{\nu_{R_H}}$. Thus, ν_{R_H} was 0.23, 0.25, 0.23 and 0.66, for A, B, C and D, respectively (Table 2). The same caution has to be considered for the validity of the ν_{R_H} values as already discussed for ν_{R_G}. In comparison with the former different $\bar{R}_G = K\bar{M}_W^{\nu_{R_G}}$ relationships, the data points on the log–log plot follow the same line, with a slope of 0.23 (Fig. 2(b)). This single scaling relationship means that the starch samples have the same hydrodynamic structure.

The dimensionless ratio $\rho = (\bar{R}_G/\bar{R}_H)$ (Table 1) is a sensitive index of structure and/or chain conformation. For A and B starches, ρ was expected to have a value in the range 0.8–1.1, characteristic of the high number of clusters in macromolecules; whereas for C and D starches, ρ was expected to increase, considering the high number of linear chains. Surprisingly, non-degraded starches showed similar experimental ρ in the 1.29–1.35 range. During the degradation process, ρ values decreased to 1 for A, B and C starches, but increased to 1.61 for starch D. The value of ρ obtained at 90 s was not in accordance with these tendencies.

Table 3
Exponent α in the power law $\Gamma \sim \mathbf{q}^\alpha$ obtained from dynamic light scattering experiments

Treatment time (s)	A	B	C	D
35	2.80	2.85	2.87	2.89
50	2.85	2.80	2.82	2.83
70	2.76	2.67	2.63	2.82
90	2.74	2.95	3.32	3.01

3.2.2. Intra-chain dynamics

As the size of the polymer was sufficiently large, it was no longer a point particle. The correlation function provided information about the detailed intramolecular motion of the polymer. We then processed the data, bearing in mind that

Table 4
Value of the prefactor $\Gamma^* = \Gamma\eta_0/(\mathbf{q}^3 k_B T)$ obtained from dynamic light scattering experiments

Treatment time (s)	A	B	C	D
35	0.038	0.037	0.045	0.055
50	0.037	0.038	0.047	0.055
70	0.038	0.045	0.044	0.057
90	0.041	0.074	0.059	0.063

the contribution of internal relaxation modes could not be neglected in this range of $\mathbf{q}\bar{R}_H$ values. Fig. 7 shows a log–log scale plot of the $\mathbf{q}$-dependence of $\Gamma/\mathbf{q}^2$, where Γ is obtained from a cumulant analysis for the four starch samples at 35 s (a straight line is obtained for each sample). The exponent α in the power-law relationship, $\Gamma \sim \mathbf{q}^\alpha$, increased from 2.80 to 2.89 with amylose content (Table 3), approaching the value of 3 expected for a fully flexible chain [28]. α decreased significantly for each starch sample, i.e. from 2.80 to 2.74 for A, from 2.85 to 2.67 for B, from 2.87 to 2.63 for C, and from 2.89 to 2.82 for D, when MDT time expanded from 35 to 90 s (Table 3). This decrease was observed as long as no aggregation occurred, i.e. for the last treatment time of samples C and D. In these cases, α increased (Table 3). The prefactor $\Gamma^* = \Gamma\eta_0/(\mathbf{q}^3 k_B T)$ was expected to show the values 0.05–0.06 and 0.045 for

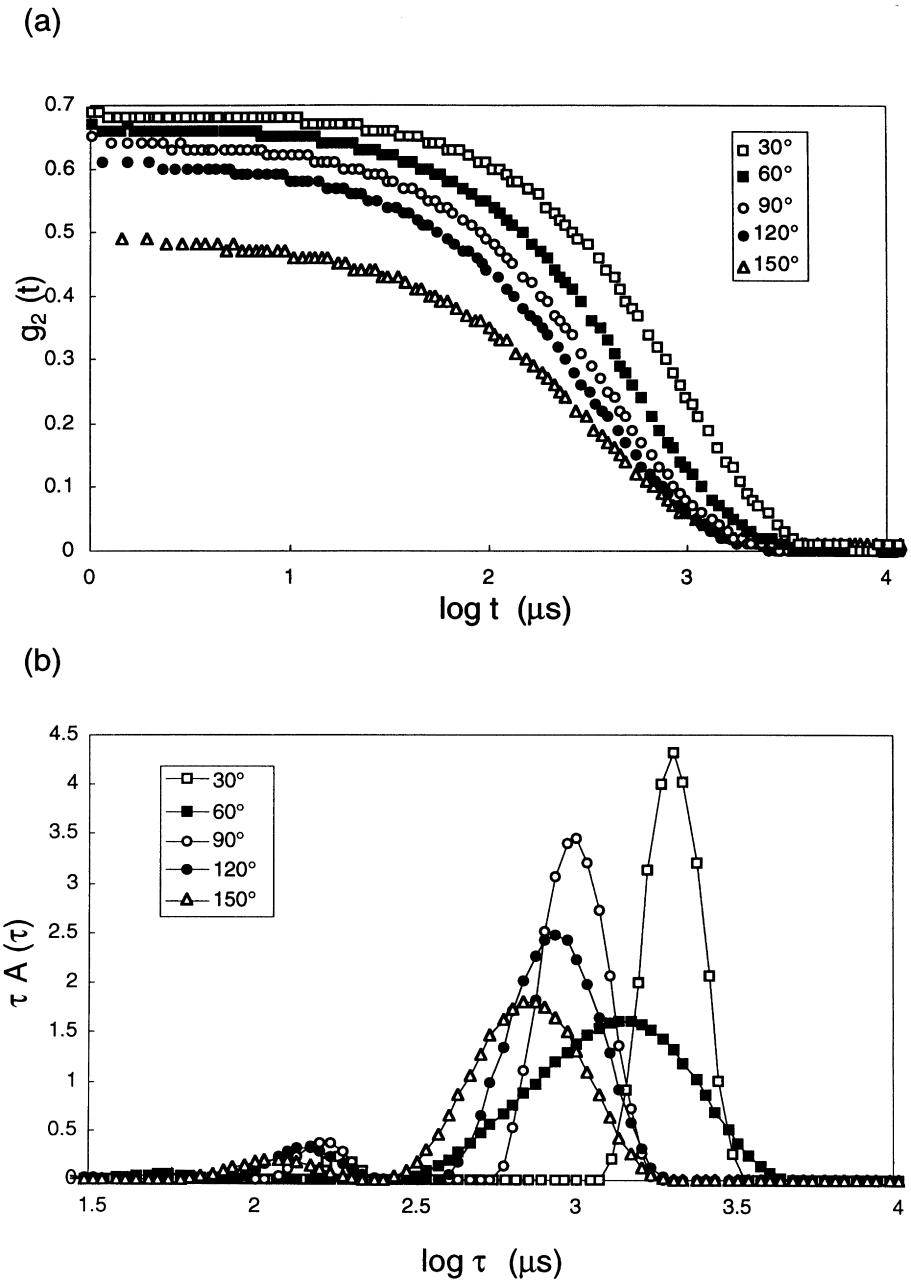

Fig. 8. Autocorrelation functions (a) and relaxation time distributions (b) at different scattering angles of sample A treated using MDT for 35 s.

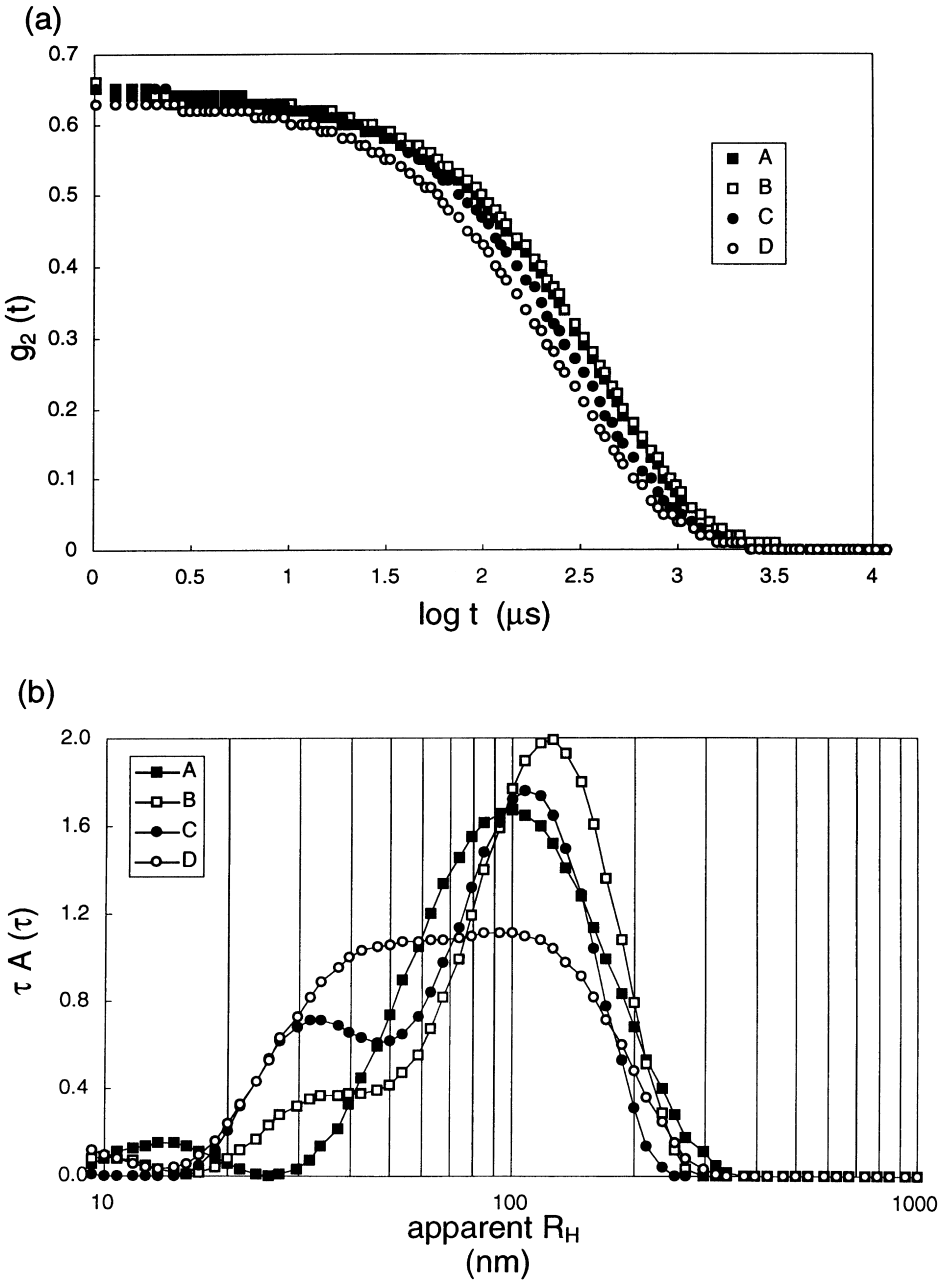

Fig. 9. Autocorrelation functions (a) and relaxation time distributions (b) of samples dissolved during 35 s and measured at 90°.

flexible chains in good and theta solvents, respectively [29]. It was found that Γ* increased from 0.037 to 0.055 with amylose content (Table 4). Surprisingly, degradation had no significant influence on Γ* (Table 4).

3.3. Relaxation time distribution

For all samples, intensity autocorrelation functions $g_2(t)$ were nearly independent of concentration (graphs not shown), which explains why the following results are all shown at the highest concentration used.

3.3.1. $\mathbf{q}^2$-dependence of the RTD

The dependence on $\mathbf{q}^2$ of the RTD obtained from experimental ACF is shown in Fig. 8. One major peak always characterised the distribution, representing at least 90% of the total area. Some other minor relaxation times were present for log $\tau < 2.5$ μs, probably because of fast internal modes of relaxation. The location of the main peak shifted to lower log τ values as $\mathbf{q}^2$ increased. However, the $\mathbf{q}^2$-dependence of the corresponding relaxation rate Γ was neither linear nor constant in this range of $\mathbf{q}$-values. This variation made it impossible to assign either a diffusional or an internal mode to this main relaxation rate. Further studies

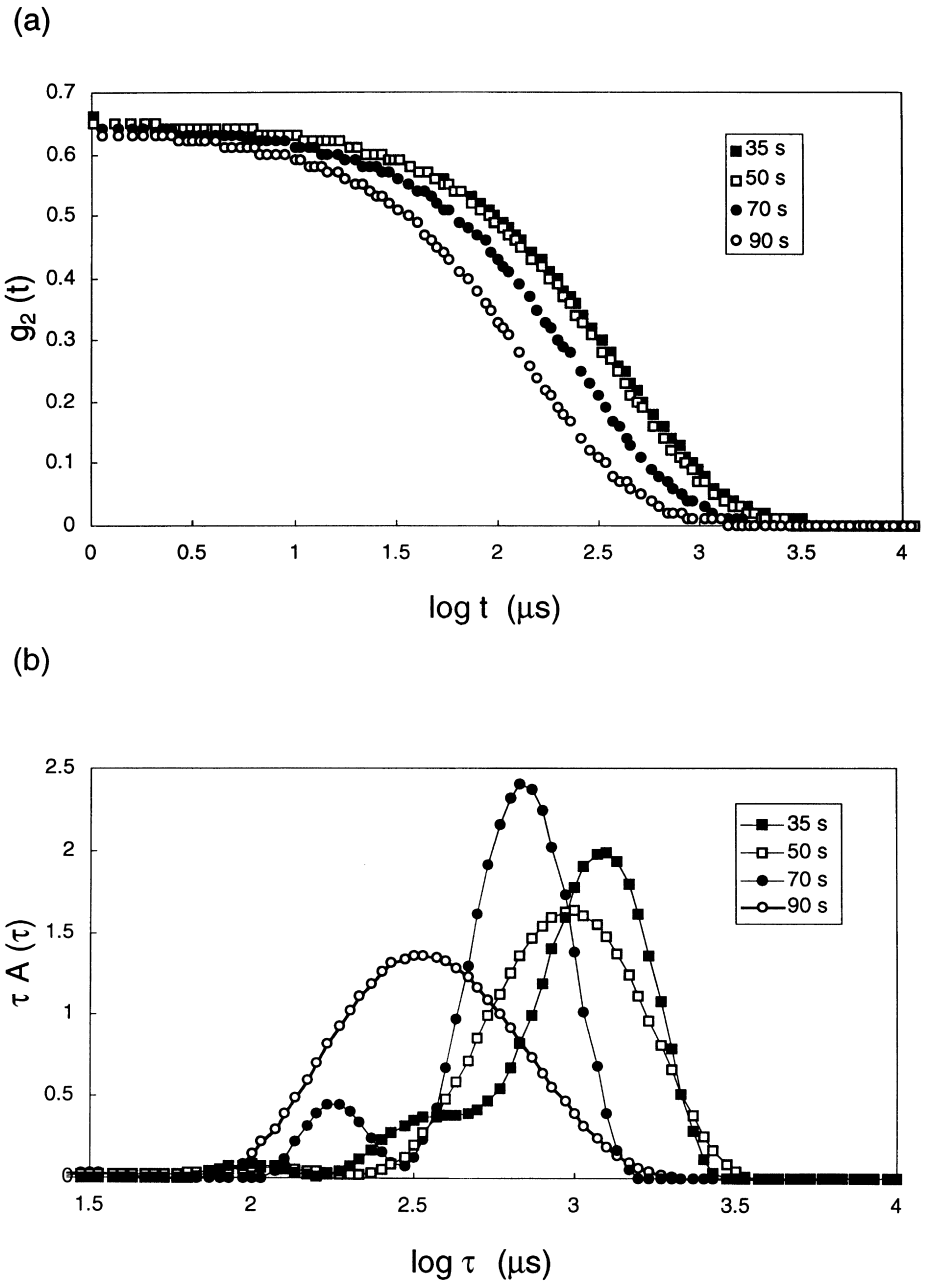

Fig. 10. Autocorrelation functions (a) and relaxation time distributions (b) of samples dissolved during the different MDT treatment times and measured at 90°.

are in progress in a range of low **q**-values, despite experimental difficulties due to excess scattering of aqueous solutions.

3.3.2. Influence of the amylose/amylopectin ratio

An interesting point concerns the influence of amylose content on the distribution of relaxation times. One consequence could relate to the estimation of amylose content in a starch sample, considering that amylose has a very small hydrodynamic radius and that an individual amylose chain is not expected to have an $\bar{R}_H$ value higher than 30 nm as compared to amylopectin [23].

Fig. 9 shows the distributions of relaxation times versus the apparent hydrodynamic radius at a scattering angle of 90°. All distributions are quite broad, with apparent R_H between 0 and 350 nm and a peak maximum at 100–150 nm. For the amylose-free sample A, only one broad peak is observed. For samples B, C, and D, bimodal distribution has been obtained, with a major peak still centred at 100–150 nm. The shoulder at lower radii (15–60 nm) increases steadily as amylose content increases.

From these data, it is possible to discriminate qualitatively by using DLS starches with different amylose contents. However, it seems difficult at present to obtain

quantitative information by DLS (for example, through a two-exponential fitting program) with the same precision as by classical iodine-based procedures.

3.3.3. Influence of treatment time

For all starches, the influence of treatment time on the intensity of autocorrelation functions $g_2(t)$ was identical, showing a shift to lower $\log t$ values as treatment time increased from 35 to 90 s (Fig. 10(a)). The distribution of relaxation times followed the same macromolecular degradation trend, i.e. the peaks were shifted to lower $\log \tau$ values (Fig. 10(b)), whereas peak intensity did not decrease steadily with treatment time. This was mainly due to the "CONTIN"-like mathematical processing in which the preferential chosen solution is perhaps not the real one when a sample with a broad distribution of molecular weight is studied.

4. Conclusions

Combined uses of laser light-scattering techniques make it possible to follow variations in the macromolecular features of starch, not only in its composition (i.e. the branched/linear content ratio) but also during a degradation process. Macromolecular features such as $\bar{M}_W, \bar{R}_G$ and $\bar{R}_H$, obtained by classical extrapolation methods to the zero scattering vector, should be considered with due caution with respect to the high $\mathbf{q}\bar{R}_G$-range studied here. Conversely, internal features such as fractal dimension d_f and the dependence of the main relaxation rate on scattering vectors are more appropriate values for discriminating between amylose-rich and amylopectin-rich starches.

The conclusions to be drawn from these analysis sets are that if the amylopectin content is the major parameter governing the behaviour of starches in solution, the contribution of amylose becomes noticeable when the weight fraction exceeds 0.5. Inter-chain aggregation resulting from amylose-rich samples is the major experimental difficulty.

Acknowledgements

One of the authors (L.A.B-P.) is grateful to the Conseil Régional des Pays de la Loire for financial support and to the Instituto Tecnológico de Acapulco for a study leave.

References

[1] Galinski G, Burchard W. Macromolecules 1995;28:2363.
[2] Thurn A, Burchard W. Carbohydr Polym 1985;5:441.
[3] Zobel HF, Stephen AM. In: Stephen AM, editor. Food polysaccharides and their applications. New York: Marcel Dekker, 1995. p. 19.
[4] French D. In: Whistler RL, BeMiller JN, Paschall EF, editors. Starch chemistry and technology. Orlando, FL: Academic Press, 1984. p. 183.
[5] Doublier JL, Colonna P, Mercier C. Cereal Chem 1986;63:240.
[6] Clark AH, Gidley MJ, Richardson RK, Ross-Murphy SB. Macromolecules 1989;22:346.
[7] Della Valle G, Colonna P, Patria A, Vergnes B. J Rheol 1996;40:347.
[8] Mauro DJ. Cereal Foods World 1996;41:776.
[9] Bello-Perez LA, Roger P, Baud B, Colonna P. J Cereal Sci 1998;27:267.
[10] Brown W, editor. Dynamic light scattering: the method and some applications. Oxford: Clarendon Press, 1993.
[11] Burchard W. In: Meuser F, Manners DJ, Seibel W, editors. Plant polymeric carbohydrates. London: Royal Society of Chemistry, 1993. p. 215.
[12] Huglin MB, editor. Light scattering from polymer solution London: Academic Press, 1972.
[13] Aberle Th, Burchard W, Vorweg W, Radosta S. Starch/Stärke 1994;46:329.
[14] Burchard W. In: Harding SE, Sattelle DB, Bloomfield VA, editors. Laser light scattering in biochemistry. London: Royal Society of Chemistry, 1992. p. 3.
[15] Galinski G, Burchard W. Macromolecules 1996;29:1498.
[16] Hanselmann R, Ehrat M, Widmer HM. Starch/Stärke 1995;46:345.
[17] Hanselmann R, Burchard W, Ehrat M, Widmer HM. Macromolecules 1996;29:3277.
[18] Planchot V, Colonna P, Saulnier L. In: Godon B, Loisel W, editors. Guide pratique d'analyses dans les industries des céréales. Paris: Lavoisier, 1996. p. 341.
[19] Paschall EF, Foster JF. J Polym Sci 1952;9:85.
[20] Stepanek P. In: Brown W, editor. Dynamic light scattering: the method and some applications. Oxford: Clarendon Press, 1993. p. 177.
[21] Takeda Y, Shitaozono T, Hizukuri S. Starch 1988;40:51.
[22] Takeda C, Takeda Y, Hizukuri S. Hizukuri. Cereal Chem 1989;66:22.
[23] Roger P, Tran V, Lesec J, Colonna P. J Cereal Sci 1996;24:247.
[24] Kodama M, Noda H, Kamata T. Biopolymers 1978;17:985.
[25] Burchard W, Cowie JMG. In: Huglin MB, editor. Light scattering from polymer solutions. London: Academic Press, 1972. p. 725.
[26] Stauffer D. Phys Rep 1979;54:1.
[27] Stauffer D, Coniglio A, Adam M. Adv Polym Sci 1982;44:103 Section III.
[28] Brown W, Nicolai T. In: Brown W, editor. Dynamic light scattering: the method and some applications. Oxford: Clarendon Press, 1993. p. 272.
[29] Trappe V, Burchard W. In: Pike ER, Abbiss JB, editors. Light scattering and photon correlation spectroscopy. NATO ASI series, 3. High technology, 40. Dordrecht: Kluwer Academic, 1997. p. 154.
[30] Schaefer DW, Hann CC. In: Pecora R, editor. Dynamic light scattering: applications of photon correlation spectroscopy. New York: Plenum Press, 1985. p. 191.